JOURNAL OF MATERIALS SCIENCE **38** (2003) 927–935

Strengthening of porous alumina bodies using carboxylate-alumoxane nanoparticles

KIMBERLY A. DEFRIEND, ANDREW R. BARRON*
Department of Chemistry, Department of Mechanical Engineering and Materials Science, and Center for Nanoscale Science and Technology, Rice University, Houston, Texas 77005, USA
E-mail: arb@rice.edu

Aqueous solutions of acetate-functionalized alumina nanoparticles (A-alumoxane), with an average particle size of 28 nm, have been used as alumina precursors for the infiltration of porous α-alumina bodies in order to produce composite structures with homo-interfaces between substrate and infiltrate. Alternatively, if metal doped-methoxy(ethoxyethoxy)acetic acid-functionalized alumina nanoparticles (M-doped MEEA-alumoxane; M = Ca, Er, La, Ti, and Y), with an average particle size of 67 nm, are used in combination with A-alumoxane, a hetero-interface is formed between substrate and infiltrate. Samples were characterized by SEM, BJH, hardness and bend strength measurements. The bulk hardness of the α-alumina substrates increases with sintering temperature, but this increase is significantly smaller than the effect of infiltration. The composite hardness generally increases with decreased average pore size although the exceptions to this trend suggest that the identity of the infiltrate is of equal or greater importance. Overall the hetero-interfaces show higher strength than the homo-interface; the latter showing only slightly better performance than high temperature sintering. For the samples fired at 1000°C, the $MgAl_2O_4/Al_2O_3$ and $CaAl_{12}O_{19}/Al_2O_3$ combinations appear to provide the greatest enhancement, with both the $LaAl_{11}O_{18}/Al_2O_3$ and $Y_3Al_5O_{12}/Al_2O_3$ hetero-interface samples show marked increase in hardness between 1000 and 1400°C. The elastic modulus and bend strength of the α-alumina substrate increases significantly for the $Er_6Al_{10}O_{24}/Al_2O_3$ and $LaAl_{11}O_{18}/Al_2O_3$ infiltrates. The identity of the hetero-interface has a significant effect on the bulk properties of the composite.

1. Introduction

Alumina based ceramics are used in a wide range of high performance applications because of their high thermal stability, and chemical and oxidation resistance [1, 2]. Unfortunately, because of the "hot press" fabrication methods commonly employed for ceramic bodies, problems with the mechanical strength of the body may arise [3, 4]. Hot pressing ceramic particles generally results in significant pore formation due to voids between the individual particles. Extensive porosity decreases the mechanical strength of the ceramic body since, for a specific material, porosity is inversely related to strength [5].

High porosity reduces the cross-sectional area of the ceramic, such that, when a load is applied, the amount of area able to carry the load is reduced; this results in low mechanical strength of the ceramic body. An additional problem associated with hot pressed alumina based ceramics is that they are often coarsely grained. Intergranular microfracture and grain dislodgment occur for coarse grained aluminas, which causes detrimental effects on mechanical properties and material performance [6]. Fracture toughness and hardness are important mechanical properties in the wear of alumina based ceramics [7]; improving toughness can improve wear resistance [8]. There are several strengthening mechanisms currently proposed: phase transformation (sintering), second particle enforcement (infiltration), fiber reinforcement [9], and the use of a pre-ceramic polymer as the binder to minimize porosity [10]. Sintering or infiltration are also possible solutions to pore reduction.

The traditional approach to porosity reduction is to heat the preform at elevated temperatures with long dwell times thus promoting grain growth, which decreases porosity. While sintering produces a dense, and in turn strong ceramic, there are drawbacks, including: possible phase changes, shrinkage, and energy consumption. As an alternative, porosity can be reduced by infiltrating the porous ceramic body with pre-ceramic materials. Pore reduction is fulfilled not through grain growth, but by adding mass to the body, which increases the density and hence strength. Infiltration may be accomplished by either vapor reactions or sol-gel techniques.

*Author to whom all correspondence should be addressed (url: www.rice.edu/barron).

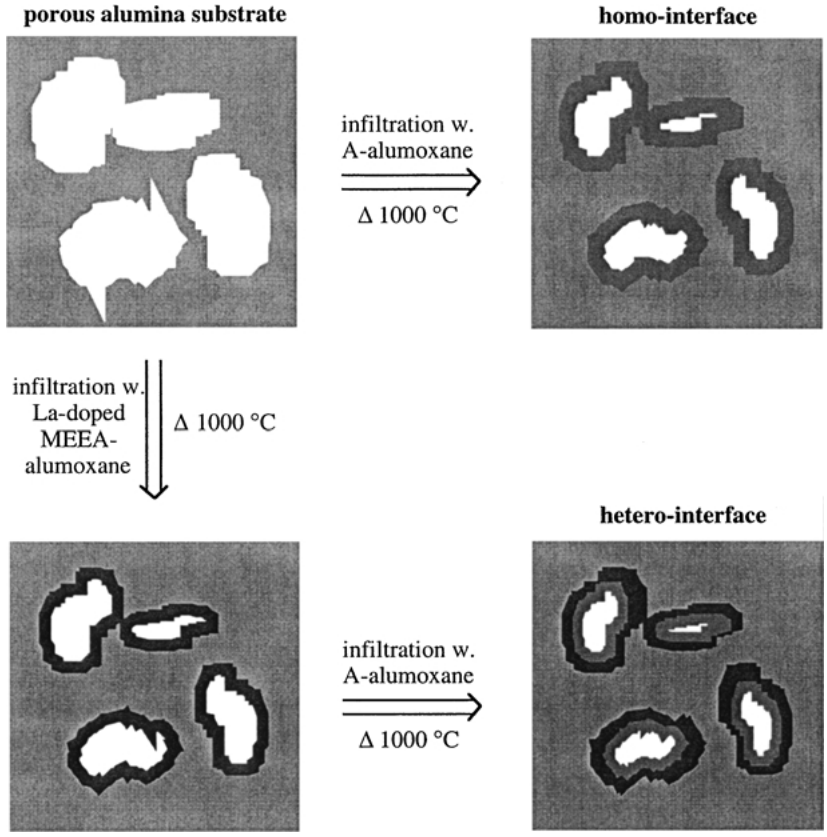

Figure 1 Schematic representation of the formation of a homo-interface through infiltration of a porous alumina ceramic body with an alumina pre-ceramic, and the formation of a hetero-interface through infiltration with a lanthanum aluminate pre-ceramic.

If an alumina body is infiltrated by an alumina forming pre-ceramic material, then upon thermolysis, alumina is formed on the inside of the pores of the alumina body. Porosity is reduced through infiltration of the ceramic body with the same ceramic material, i.e., a homo-interface is formed between substrate and infiltrate (Fig. 1). Alternatively, if upon thermolysis the pre-ceramic forms a material with a different chemical composition than the substrate, a hetero-interface is formed between substrate and infiltrate (Fig. 1). The hetero-interface can be formed with a material that binds weakly to the inside of the porous body, so to deflect cracks and reduce crack propagation upon impact, which is needed to develop tough, strong ceramics [8, 11, 12].

For infiltration to be successful, the infiltrate should have certain requirements. To strengthen the whole porous ceramic body, the infiltration process should be continuous throughout [13]. It is desirable for the pre-ceramic to dissolve in aqueous media for environmentally benign processing. For porous bodies with relatively small pores, a small particle size is needed to successfully infiltrate and decrease porosity. High ceramic yield is also desirable when trying to deposit the greatest amount of mass for near pore reduction. Solution infiltration offers a simpler processing technique than some vapor methods. The usual method of infiltration from solution is the sol-gel method. The ceramic yield for sols is often low causing extensive shrinkage and cracking. Furthermore, the typical alumina-based sol has a large particle size distribution and uses organic solvents or strong mineral acids [1, 14].

We have previously demonstrated that water soluble carboxylate-substituted alumina nanoparticles (carboxylate-alumoxanes) may be readily prepared with a narrow particle size distribution and a high ceramic yield [10]. In addition, we have shown that these nanoparticles may be reacted with metal complexes to form metal doped nanoparticles, by way of a transmetalation reaction, upon thermolysis forming mixed metal oxides [15, 16]. Furthermore, we have found that aqueous solutions of carboxylate-alumoxanes nanoparticles may be used for the fabrication of highly uniform aluminate interface coatings for SiC and sapphire fiber reinforced ceramic matrix composites [17, 18] as well as for the surface repair of porous and damaged alumina bodies [19]. Herein we report the application of alumoxanes nanoparticles and metal-doped alumoxanes nanoparticles for the strengthening of porous alumina bodies.

2. Experimental procedure

2.1. General

Research grade boehmite (Catapal-B) was provided by Vista Chemical Company. Porous hot pressed α-Al_2O_3 discs were obtained from Refractron Technologies Corp. (Newark, NJ). Acetic acid (A-H), methoxy-(ethoxyethoxy)acetic acid (MEEA-H, **I**) and $La(acac)_3$ (Fisher Scientific, Fluka and Strem Chemical, respectively) were used without further purification. MEEA-alumoxane, A-alumoxane, and Ca-, Er-, La-, Ti-, and Y-doped MEEA-alumoxanes were prepared by previously published methods [15, 16]. Standard aqueous

solutions of 1% wt A-alumoxane and 10% wt La-MEEA-alumoxane were prepared by stirring the alumoxane in DI water until completely dissolved and then centrifuged to 3500 rpm for 1 hour to remove excess air bubbles and unreacted boehmite. The solutions may be stored indefinitely until time of use.

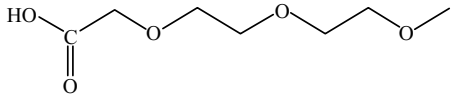

(I)

Scanning electron microscopy studies were performed on a Phillips XL-30 ESEM at 15 kV. The samples were mounted on carbon tape and sputter coated with gold. Cross-sections of the infiltrated ceramics were performed to address the success of full infiltration. SEM images of the surface determined the surface roughness, and the progress of infiltration. Electron probe microanalysis was performed on a Cameca SX50 Electron Microprobe using imaging techniques of secondary electron emission (topology, morphology), and wavelength dispersive X-ray distribution maps (elemental maps). The elemental maps were used to determine uniformity of infiltration and the location of the lanthanum and aluminum on the interior to confirm capillary infiltration had occurred. Surface area analysis was performed on Coulter SA 3100 BET analyzer using N_2 gas adsorption. The samples were outgassed under nitrogen for 1 hour at 200°C before analysis. Microindention testing was performed on a Micromet microhardness tester. Load weights varied with the sample. The hardness was determined by inserting the load weight and the area of indention into the Vicker's equation: $H_v = 1.85444(P/d^2)$ where P is the load in Kg and d^2 is the area of indention in mm^2. Five indentation measurements were performed on each sample. Powder X-ray diffraction patterns of A-alumoxane and La-doped MEEA-alumoxane were determined by using a Siemens Diffractometer. The detected patterns confirm the crystalline α-Al_2O_3 and $LaAlO_3$ phases. Samples of A-alumoxane and La-doped MEEA-alumoxane were fired to 1400°C with holding times of 5 hours before analysis. The elastic modulus and bending strength determination was conducted on Satec Systems Instron 5565 with a crosshead speed of 0.2 mm/min and loading span of 20 mm. The sample size was 25 ± 1.5 mm $\times$ 6.5 ± 1.2 mm $\times$ 2 ± 0.3 mm according to ATSM standard C1161-94. To obtain correct sample dimensions the samples were sliced with a diamond blade saw with water as the lubricant. A minimum of ten measurements were made for each sample condition.

2.2. Heat treatment of porous α-Al_2O_3 substrate

An α-alumina substrate was washed in acetone and heated to 600°C to remove surface grease. The substrates were then sintered to 1400°C over 7 hours with a dwell time of 5 or 12 hours. These samples replicate sintering a hot pressed substrate to increase grain growth and decrease porosity.

2.3. Homo-interface: Infiltration of A-alumoxane into porous α-Al_2O_3 substrates

Infiltration by a 1% wt solution of A-alumoxane was used to form the homo-interface within the pores of the α-Al_2O_3 ceramic body. Substrates were washed in acetone and heated to 600°C to remove surface grease. Once cooled to room temperature, they were then placed in the A-alumoxane solution, making sure the solution did not cover the top surface of the samples. This procedure was to ensure that infiltration occurred only by capillary action. Infiltration was continued until the top surface was covered with the solution ensuring complete and reproducible infiltration. A schematic representation of the infiltration process is shown in Fig. 2. Infiltration time was 1 hour under vacuum. The samples were allowed to air dry for 1 day before firing to 1000°C with a 5 hour dwell time. This infiltration, air dry, and firing sequence was conducted 10 times. One set of samples was subsequently sintered to 1400°C with a 5 hour dwell time.

2.4. Hetero-interface: Infiltration of lanthanum-doped MEEA-alumoxane and A-alumoxane into porous α-Al_2O_3 substrates

A 10% wt La-MEEA-alumoxane solution was used to form the hetero-interface. Substrates were washed in acetone and heated to 600°C to remove surface grease.

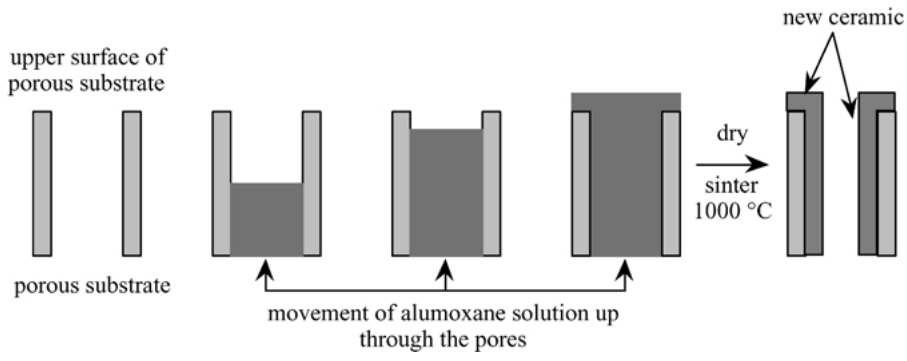

Figure 2 Schematic representation of cappilary infiltration process.

TABLE I Summary of synthetic methods and the physical data for the ceramic products from the infiltration of alumoxane and metal-doped alumoxane into porous alumina substrates

Infiltrate	T (°C)	Time (hours)	Average pore diameter (nm)	H_v surface[a]	H_v bulk[a,b]	Elastic modulus (10^3 MPa)[a]	Bend strength (MPa)[a]
None	n/a	n/a	47	370 ± 20	310 ± 40	28 ± 1	90 ± 10
None	1400	5	48	400 ± 40	490 ± 50	33 ± 1	90 ± 10
None	1400	12	27	470 ± 40	550 ± 30	57 ± 1	170 ± 20
Al_2O_3	1000	5	36	350 ± 20	630 ± 20	34 ± 1	100 ± 10
Al_2O_3	1400	5	37	500 ± 30	660 ± 40	37 ± 3	90 ± 10
$LaAlO_3/Al_2O_3$	1000	5	35	260 ± 15	700 ± 30	37 ± 2	100 ± 10
$LaAlO_3/Al_2O_3$	1400	5	27	620 ± 30	740 ± 30	36 ± 1	120 ± 10
$CaAl_{12}O_{19}/Al_2O_3$	1000	5	46	130 ± 8	1100 ± 50	33 ± 1	110 ± 10
$CaAl_{12}O_{19}/Al_2O_3$	1400	5	13	470 ± 20	960 ± 30	41 ± 5	140 ± 20
$Er_6Al_{10}O_{24}/Al_2O_3$	1000	5	21	200 ± 5	880 ± 40	50 ± 10	140 ± 20
$Er_6Al_{10}O_{24}/Al_2O_3$	1400	5	7	250 ± 20	880 ± 10	60 ± 10	140 ± 10
$LaAl_{11}O_{18}/Al_2O_3$	1000	5	18	290 ± 8	870 ± 60	60 ± 10	150 ± 20
$LaAl_{11}O_{18}/Al_2O_3$	1400	5	30	280 ± 40	1300 ± 100	60 ± 10	130 ± 10
$MgAl_2O_4/Al_2O_3$	1000	5	35	220 ± 10	1170 ± 80	42 ± 4	100 ± 10
$MgAl_2O_4/Al_2O_3$	1400	5	24	260 ± 30	1120 ± 40	40 ± 10	100 ± 20
Al_2TiO_5/Al_2O_3	1000	5	41	275 ± 30	570 ± 30	41 ± 2	130 ± 10
Al_2TiO_5/Al_2O_3	1400	5	23	410 ± 60	560 ± 30	53 ± 1	180 ± 5
$Y_3Al_5O_{12}/Al_2O_3$	1000	5	54	430 ± 30	631 ± 50	33 ± 1	130 ± 20
$Y_3Al_5O_{12}/Al_2O_3$	1400	5	21	490 ± 20	900 ± 20	41 ± 5	120 ± 30

[a]Average values over five samples.
[b]Average values over five samples in both cross section and internal horizontal plane.

Once cooled to room temperature, substrate samples were placed in the La-doped MEEA-alumoxane solution, and vacuum infiltrated for 1 hour. The samples were allowed to dry in air before firing to 1000°C with a 5 hour dwell time. The infiltration/fire sequence was carried out three times, after which infiltration was performed using a 1% wt solution of A-alumoxane (for 1 hour). The samples were dried in air before firing to 1000°C with a 5 hour dwell time. One set of samples was subsequently sintered to 1400°C with a 5 hour dwell time.

Infiltration by other metal-doped MEEA-alumoxane solutions was performed in a manner analogous to that for $LaAlO_3$. A summary of metal dopants and reaction conditions is provided in Table I.

2.5. Synthesis of magnesium doped MEEA-alumoxane and $MgAl_2O_4$

To a solution of MEEA-alumoxane (10 g) in water (500 mL) was added a stoichiometric quantity of $Mg(acac)_2$ (15.5 g) dissolved in the same solvent. The reaction was stirred at room temperature for 3 h followed by removal of volatiles under vacuum. The solid obtained was washed with Et_2O to yield the Mg-doped MEEA-alumoxane, which was dried in air. In order to characterize the thermolysis products of the Mg-doped MEEA-alumoxane, a sample was converted to $MgAl_2O_4$ according to the following thermal series: single step (ca. $50°C \cdot min^{-1}$) temperature ramp from 25°C to 1000°C in air followed by calcination for 4 h; temperature ramp to 1400°C at $2°C \cdot min^{-1}$ in air followed by calcination for minimum 4 h. XRD confirmed the formation of $MgAl_2O_4$ (JCPDS #21-1152).

2.6. Rate of infiltration

Refractron^{TM} α-alumina support was sliced to specific dimensions, 25 ± 1.5 mm $\times$ 6.5 ± 1.2 mm $\times$ $2 \pm$ 0.3 mm, and weighed before infiltration. A-alumoxane of 1 wt% was used, and 0.1 M HCl or 0.1 M NaOH was used to alter the pH. The sliced samples were placed in the alumoxane solution and allowed to vacuum infiltrate. The first study looked at the rate of infiltration over a period of 5 hours. From this, it was determined that the rate does not change after 1 hour. Therefore, samples were infiltrated for 1 hour, with weight measurements taken every 10 minutes.

3. Results and discussion

Refractron^{TM} α-alumina substrates are coarse grained with average grain size of 100–500 nm, for which full characterization is provided previously [20]. The average pore size (94 nm) and surface area ($3.5\ m^2 \cdot g^{-1}$) of these substrates makes them a convenient candidate for our infiltration studies. Nitrogen absorption revealed a broad distribution of pores with a maximum pore size over 150 nm (see Fig. 3). In comparison, the A-alumoxane and La-doped MEEA-alumoxane nanoparticles (28 and 67 nm, respectively [21]) are sufficiently small to enable easily infiltrate. To provide a comparison with the homo and hetero-interface infiltrations, samples of the α-alumina substrates were sintered to 1400°C for 5 and 12 hours (see Table I).

Samples of the α-alumina substrates were infiltrated with A-alumoxane such that thermolysis (1000°C) resulted in the formation of a γ-alumina infiltrate (2nd phase) and the reduction of porosity. The infiltration by alumina does not provide any chemical reinforcement, i.e., while grain boundaries will exist between the substrate and the infiltrate, the interface is homophasic. In contrast, infiltration with the doped alumoxanes (followed by the smaller sized undoped alumoxane) is designed to result in the creation of a mixed metal interphase (1st infiltrate) between the alumina of the substrate and the 2nd infiltrate. For each

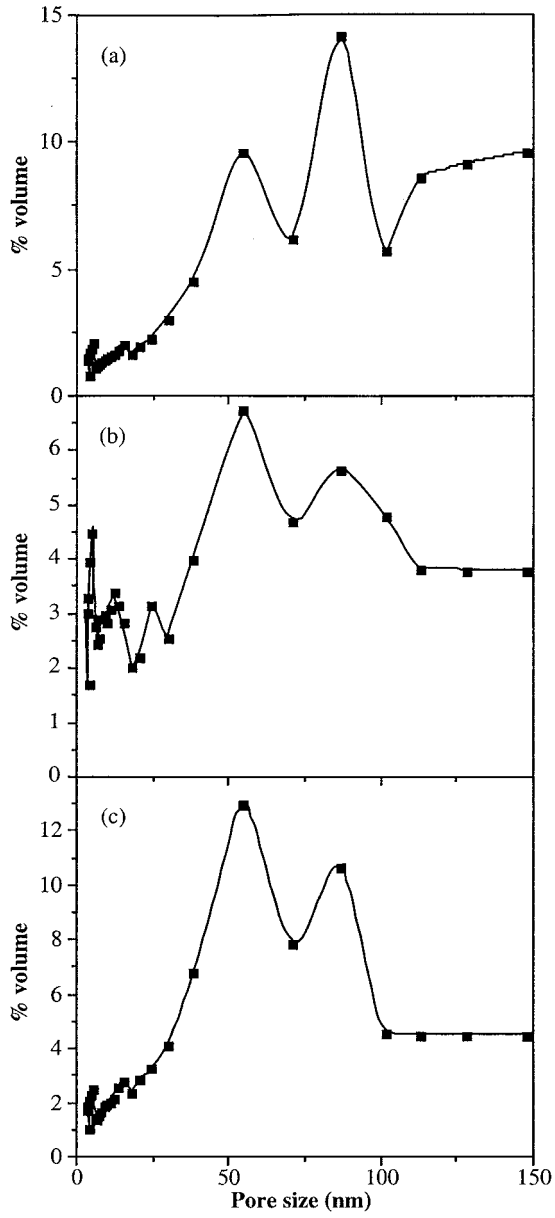

Figure 3 Nitrogen adsorption BJH pore volume distribution of (a) the as received α-alumina support, (b) after sintering to 1400°C for 12 hours, and (c) after infiltration with La-doped MEEA-alumoxane/A-alumoxane and sintering at 1000°C for 5 hours to give a $LaAlO_3/Al_2O_3$ composite.

infiltration experiment, samples were heated to 1000°C or 1400°C. Our previous work has shown that the alumoxane all decompose to a ceramic at temperatures significantly below 1000°C. However, some materials are still amorphous at this temperature or undergo a phase transformation among 1000 and 1400°C, so samples for each infiltrate were also sintered subjected to a second sintering to 1400°C. The choice of the 2nd mixed metal phase was based upon our desire to investigate the effect of (a) isomorphous materials with different chemical compositions (e.g., $LaAlO_3$ versus Al_2O_3), (b) layered versus non-layered materials (e.g., $LaAl_{11}O_{18}$ versus $LaAlO_3$), and (c) phases that undergo crystallization or phase changes between 1000 and 1400°C.

For each sample the pore size distribution and average pore size were determined by BJH measurements. Hardness measurements were made of bulk and surface of each sample. Two separate measurements were made to determine the bulk hardness; the vertical plane after cross sectioning and the internal horizontal plane after cleavage within the plane of the substrate. Finally, the elastic modulus and bending strength were obtained. In each case, measurements were made for at least five samples and an average taken. Table I provides a summary of all the analytical data.

Sintering the, as received, α-alumina substrate to 1400°C for 5 hours does not result in a significant change in the average pore diameter, however, based upon the pore size distribution there is a decrease in the largest pores (>120 nm). As expected longer sintering times (12 h) result in a noticeable decrease in the average pore size, again, mainly being due to the closing of the largest pores and the creation of smaller pores (ca. 20 nm), see Fig. 3b. As was noted above, grain growth of the hot pressed ceramic particles is responsible for the decrease in porosity. A comparison of the SEM of an α-alumina substrate before and after sintering for 12 h to 1400°C is consistent with modest grain growth (Fig. 4).

The SEM images of α-alumina substrates infiltrated with the alumoxane (before thermolysis) show the presence of significant additional material (Fig. 5). Although, there is some shrinkage upon thermolysis and sintering due to the loss of the organic component of the alumoxanes, the ceramic infiltrate is clearly observed. Cross sectional and surface SEM images confirm capillary infiltration. Thus, it appears that the interior pores are lined with the infiltrate ceramic for which a uniform distribution of the infiltrate may be confirmed, in the case of the hetero-infiltrates, by the appropriate elemental map (e.g., Fig. 6). Where the substrate has

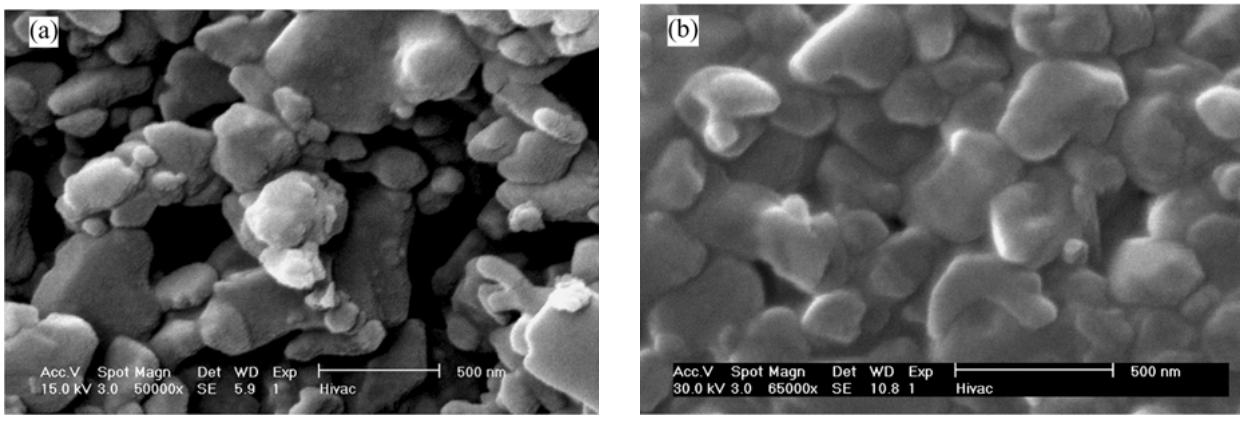

Figure 4 SEM images of the surface of (a) untreated α-alumina support and (b) after sintering to 1400°C for 12 hours.

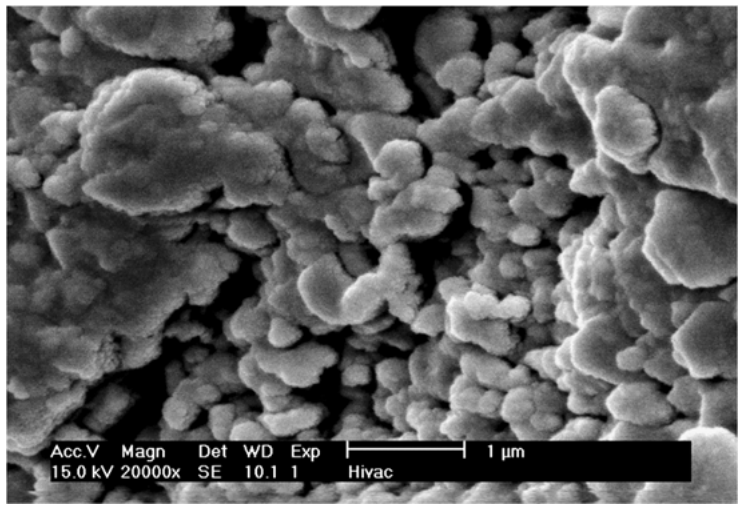

Figure 5 Cross-sectional SEM image of an α-alumina substrate infiltrated with A-alumoxane prior to thermolysis and sintering.

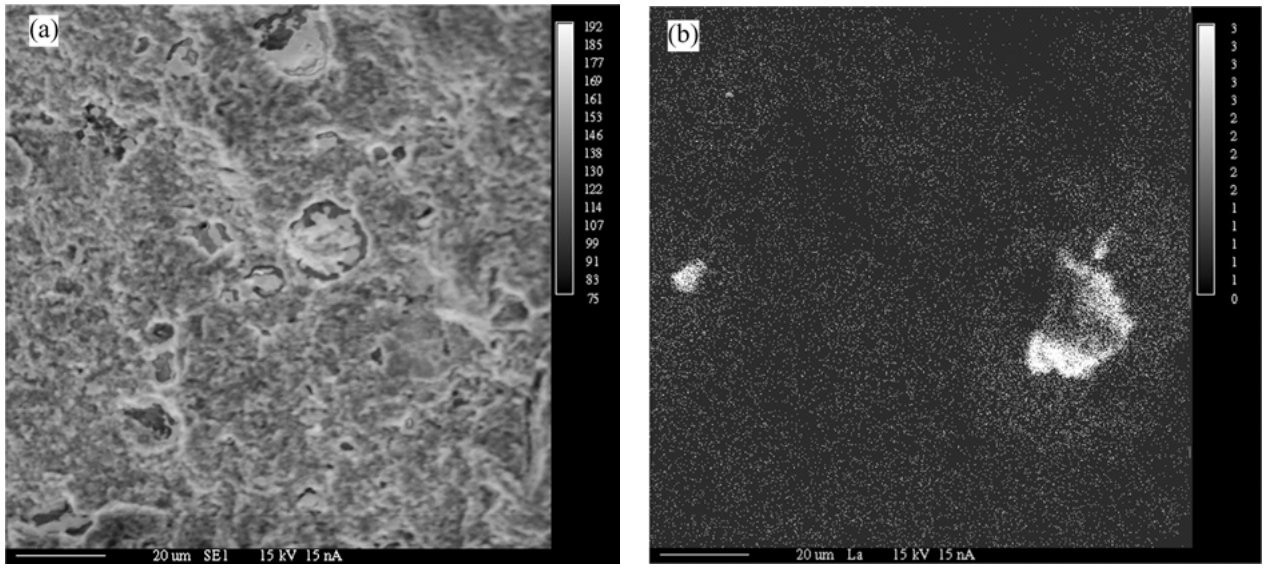

Figure 6 SEM of a cleaved α-alumina substrate infiltrated with $LaAlO_3/Al_2O_3$ heterointerface (a) and (b) the associated lanthanum elemental map.

macroscopic cracks or defects, the infiltration appears to successfully fill the entire void, see Fig. 7. For the hetero-infiltrates the crystalline phase of the infiltrate is confirmed by XRD in comparison with prior results [16].

Infiltration with either A-alumoxane, or a combination of doped MEEA-alumoxane and A-alumoxane, results in a modest but significant decrease in the average pore size (see Table I). Infiltration with the alumoxanes appears to significantly reduce the fraction of pores above 90 nm (Fig. 3c). Sintering the infiltrated samples to 1400°C further reduces the average pore size, however, it appears that some additional porosity between 1–10 nm is created due to the infiltrate itself (Table I).

The bulk hardness of the α-alumina substrates increases with sintering temperature and time. The increase is significantly smaller than the effect of infiltration, see Table I and Fig. 8. There appears to be no clear trend between the average pore size and the bulk hardness of the composites. The hardness generally increases with decreased average pore size although the exceptions to this trend suggest that the identity of the infiltrate is of equal or greater importance. We note, however, that the hardness is related more to the distribution of pore sizes rather than the average.

Overall it is worth noting that the hetero-interfaces show higher strength than the homo-interface; the latter showing only slightly better performance than high temperature sintering. For the samples fired at 1000°C, the $MgAl_2O_4/Al_2O_3$ and $CaAl_{12}O_{19}/Al_2O_3$ combinations appear to provide the greatest enhancement, with the $Er_6Al_{10}O_{24}/Al_2O_3$ and $LaAl_{11}O_{18}/Al_2O_3$ infiltrates also offering significant results (Fig. 9). Thus, the phase of the infiltrate appears to be important in determining the hardness as opposed to the infiltration *per se*.

Generally, sintering the infiltrated sample at 1400°C does not provide significant change, however, both the $LaAl_{11}O_{18}/Al_2O_3$ and $Y_3Al_5O_{12}/Al_2O_3$ heterointerface samples show marked increase in hardness between 1000 and 1400°C (Fig. 9). We have previously reported that firing Y-doped MEEA-alumoxane nanoparticles to 1000°C for 4 h yields a white solid identified by XRD as YAG (JCPDS #33-0040), but that further sintering to 1400°C drastically increases crystallinity and grain growth. We have also noted

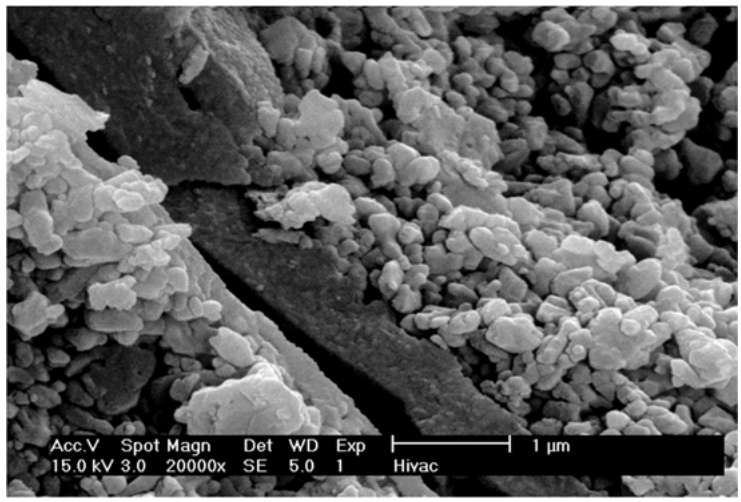

Figure 7 Cross-sectional SEM image of an α-alumina substrate infiltrated with A-alumoxane after sintering to 1000°C showing the infiltration of a macroscopic crack.

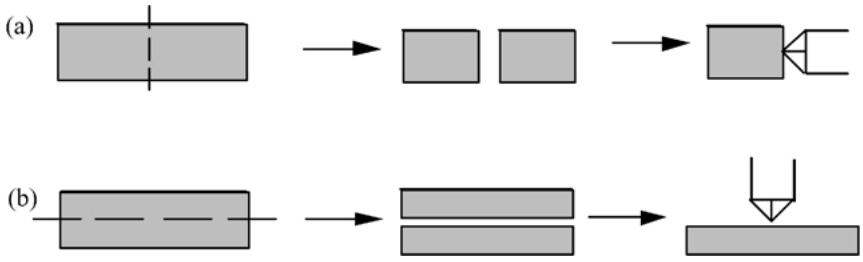

Figure 8 Pictorial representation of the measurements made to determine the bulk hardness by cross-sectioning the sample (a) along the internal vertical plane and (b) along the internal horizontal plane.

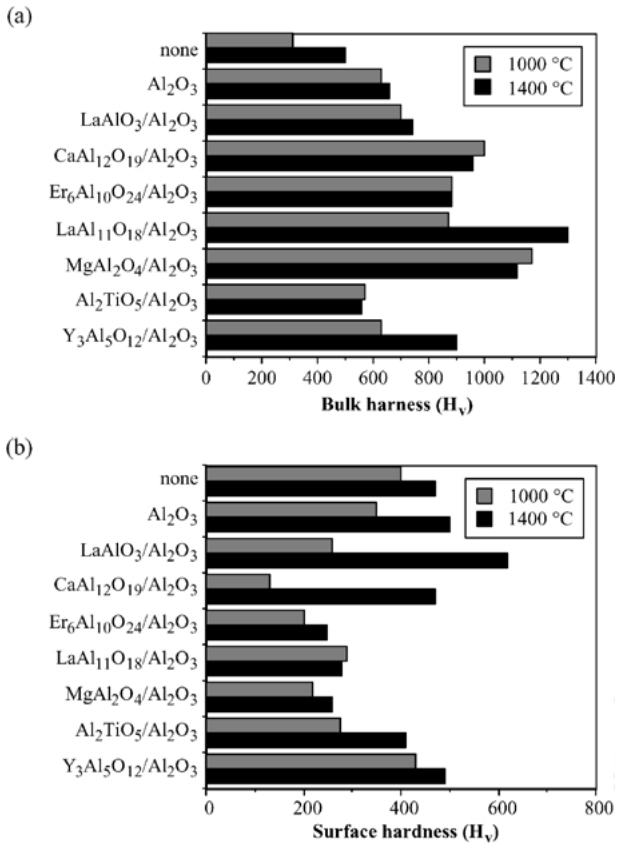

Figure 9 Plot of (a) bulk and (b) surface hardness (H_v) for the α-alumina substrate and infiltrated samples heated to 1000°C and 1400°C.

that extended sintering of La-doped MEEA-alumoxane at 1400°C produces highly crystalline phase pure $LaAl_{11}O_{18}$(JCPDS #33-0699). We have not observed significant grain growth for the other mixed metal oxides prepared from doped alumoxanes, over the temperature and times studied herein. It is possible that the statistically significant increase in bulk hardness observed for both the $LaAl_{11}O_{18}/Al_2O_3$ and $Y_3Al_5O_{12}/Al_2O_3$ hetero-interface samples upon sintering to 1400°C are due to rapid grain growth.

Whereas the hardness of the surface and interior of the α-alumina substrate are similar (even after sintering), there is a significant difference between the values obtained for the infiltrated samples. As may be seen from Fig. 9b, the surface hardness for the infiltrated samples fired to 1000°C is lower than the substrate. The reason for this decrease may be obtained from the SEM images and AFM data for the surface. As is exemplified in Fig. 2, the surfaces of the infiltrated samples consist of a "spongy" layer of new material with a small grain size. This "spongy" layer is clearly seen in cross section (Fig. 10) and is approximately 5 μm in thickness. The coating is formed during infiltration as a result of capillary action that forced the alumoxane solution through the entire interior of the ceramic body until it reached the top, where it spilt onto the surface, see Fig. 2. We have previously reported that surface coatings may be applied to porous ceramic substrates for membrane [20] or surface repair [19] applications.

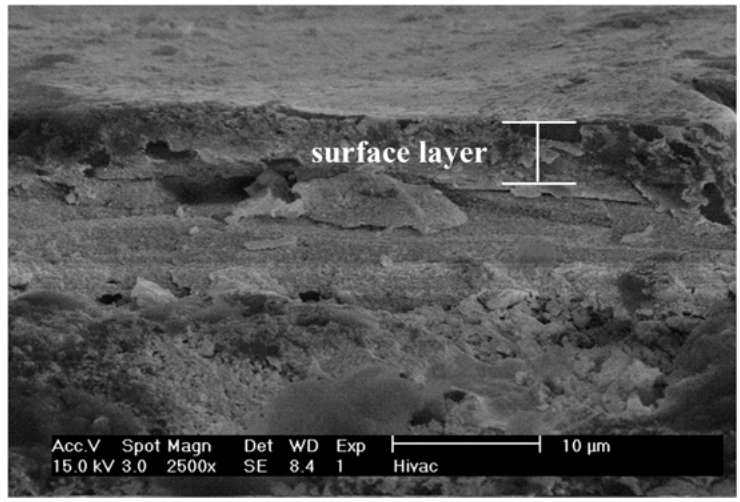

Figure 10 Cross section SEM image of the spongy surface layer formed due to capillary infiltration.

A comparison of the surface and bulk hardness (H_v) for the α-alumina substrate and infiltrated samples heated to 1400°C (Fig. 9) shows that while the hardness of the new material increases with sintering temperature, it never approaches that of the same sample's interior (bulk hardness). This suggests that the increases in hardness observed for the hetero-interface composites is a function of the composite structure rather than the infiltrate materials alone.

The modulus and bend strength of the α-alumina substrate increases slightly with sintering and infiltration (Table I); significant changes are only observed for the $Er_6Al_{10}O_{24}/Al_2O_3$ and $LaAl_{11}O_{18}/Al_2O_3$ infiltrates and to a lesser extent Al_2TiO_5/Al_2O_3. A comparison of the modulus and bend strengths for samples with no infiltration, homo-infiltration and hetero-infiltration of either $LaAlO_3/Al_2O_3$ or $LaAl_{11}O_{18}/Al_2O_3$ (Fig. 11) demonstrates the effects of infiltration and infiltration phase. From Fig. 11a it can be seen that while homo-infiltration and hetero-infiltration with $LaAlO_3/Al_2O_3$ show little effect as compared to the base substrate, the use of $LaAl_{11}O_{18}/Al_2O_3$ infiltration results in a 50% and 100% increase in bending strength and elastic modulus, respectively. Thus, the identity of the hetero-interface has a significant affect on the bulk properties of the composite.

To determine the time needed for the infiltration of carboxylate-alumoxanes into a porous alumina substrate, measurements of the substrate's weight gain over time were performed at varying pH ranges; altering the pH of the A-alumoxane solution will change the particle size of the resulting alumoxane [21]. For acidic solutions, the particle size decreases, however, as the pH increases, the particles agglomerate (Fig. 12).

Each solution was allowed to infiltrate into the substrate for 5 hours, taking weight measurements every 30 minutes. It was found that after 1 hour, the weight did not increase significantly, therefore, the amount of mass the substrate can obtain at any given infiltration is maximized after 1 hour. During the 1 hour sequence, however, there is a steady increase in weight. Additionally there is also a change in the rate of infiltration as the particle size changes. As the particle size increases, the rate of infiltration decreases. The ability of the larger particles to infiltrate into the substrate is hindered, slowing the rate of infiltration of those particles into the substrate. As the particle size decreases, upon addition of acid, the rate decreases. The ability of the smaller particle sizes to infiltrate into the large pores of the substrate increases, but due to the lower mass associated with smaller particles, the rate of infiltration determined by the rate of mass change has decreased. The particle size producing the optimum rate of infiltration into the porous substrate was determined to be 50 nm (see Fig. 13).

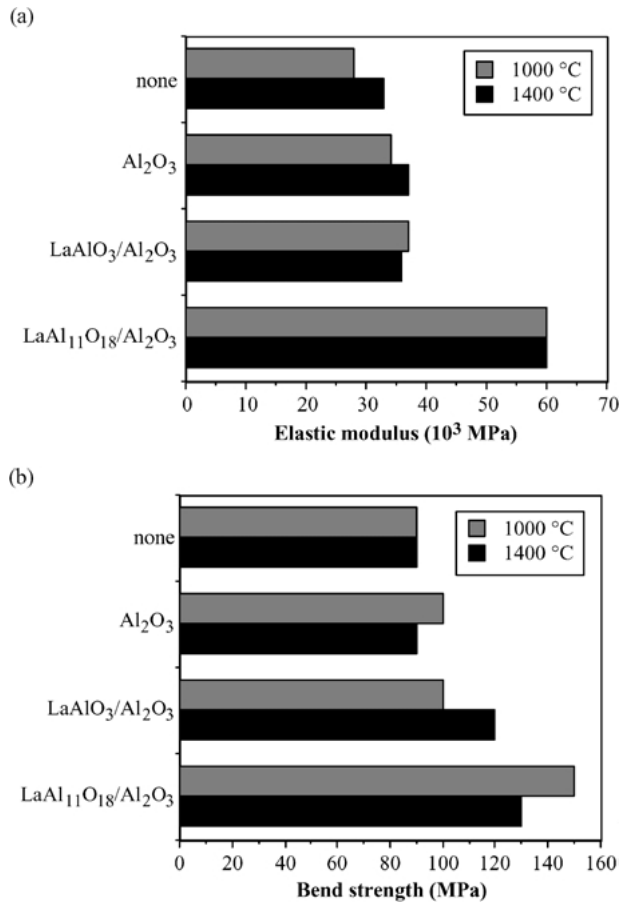

Figure 11 A comparison of the (a) elastic modulus (10^3 MPa) and (b) bend strength (MPa) for the α-alumina substrate and lanthanum aluminate infiltrated samples heated to 1000 and 1400°C.

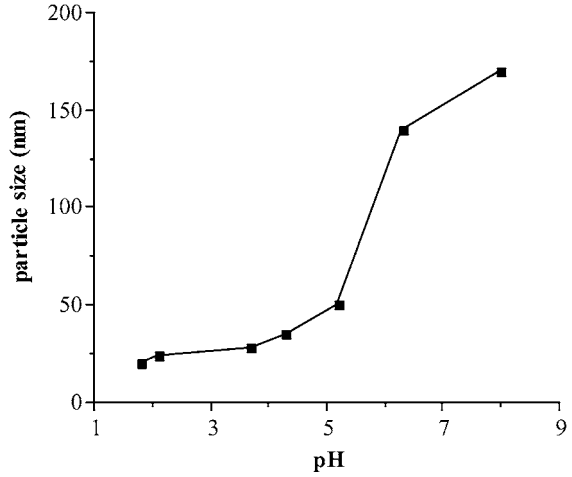

Figure 12 Plot of particle size as a function of pH for A-alumoxane.

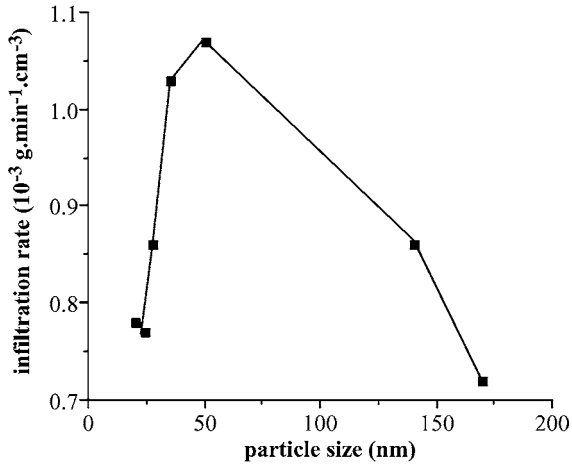

Figure 13 Plot showing the optimum particle size for maximization of infiltration rate of A-alumoxane into a porous α-alumina substrate.

4. Conclusions

Our approach to decrease porosity is forming the Al_2O_3 homo-interface or the $LaAlO_3$ hetero-interface by infiltrating with A-alumoxane or La-MEEA-alumoxane nanoparticles, respectively. The ability for the alumoxane nanoparticles, either A-alumoxane or La-MEEA-alumoxane, to infiltrate into to porous body allows for the formation of the homo or the hetero-interface, and aids in decreasing porosity and increasing strength.

Elastic modulus and bending strength also differ between a hot pressed ceramic, traditional method, and our method of decreasing porosity. Strength of the traditionally treated sample increased in strength compared to not firing, and is comparable to the formation of the homo-interface. However, the hetero-interface sample had the greatest increase in strength. The infiltration of the hetero layer weakly bonds to the inside of the pores. This enables for cracks to deflect and debonding when a stress is applied so the sample will not collapse and fail. Strength of the traditional method is comparable to the homo-interface, but the homo method used a lower firing temperature and shorter dwell time than the traditional route.

Acknowledgments

Financial support for this work was provided by the Robert A. Welch Foundation and the National Aeronautics and Space Administration.

References

1. E. L. COURTRIGHT, *Ceram. Eng. Sci. Proc.* **12** (1991) 1725.
2. C. K. NARULA, J. E. ALLISON, D. R. BAUER and H. S. GANDHI, *Chem. Mater.* **8** (1996) 984.
3. W. D. KINGERY, H. K. BOWEN and D. R. UHLMANN, *Introduction to Ceramics*, 2nd ed. (Wiley, New York, 1976) Chapter 1.
4. D. W. RICHERSON, in "Modern Ceramic Engineering" (Marcel Dekker, New York, 1992) p. 373.
5. A. S. WAGH, J. P. SINGH and R. B. POEPPEL, *J. Mater. Sci.* **28** (1993) 3589.
6. S. M. WIEDERHORN and B. J. HOCKEY, *ibid.* **18** (1983) 766.
7. A. G. EVANS and T. R. WILSHAW, *Acta Metall.* **24** (1979) 939.
8. J. F. BELL and P. S. ROGERS, *Mater. Sci. Technol.* **3** (1987) 807.
9. A. G. EVANS, *J. Am. Ceram. Soc.* **73** (1990) 187.
10. R. L. CALLENDER, C. J. HARLAN, N. M. SHAPIRO, C. D. JONES, D. L. CALLAHAN, M. R. WIESNER, R. COOK and A. R. BARRON, *Chem. Mater.* **9** (1997) 2418.
11. P. E. D. MORGAN and D. B. MARSHALL, *Mater. Sci and Eng.* **A162** (1993) 15.
12. M. Y. HE and J. W. HUTCHINSON, *Int. J. Solids Structures* **25** (1989) 1053.
13. W. C. MOFFATT and H. K. BOWEN, *J. Mater. Sci.* **24** (1989) 3984.
14. D. R. CORBIN, J. B. PARISE, U. CHOWDHRY and M. A. SUBRAMANIAN, *Mater. Res. Soc., Symp. Proc.* **233** (1991) 213.
15. A. KAREIVA, C. J. HARLAN, D. B. MACQUEEN, R. COOK and A. R. BARRON, *Chem. Mater.* **8** (1996) 2331.
16. R. L. CALLENDER and A. R. BARRON, *J. Am. Ceram. Soc.* **83** (2000) 1777.
17. *Idem.*, *J. Mater. Res.* **15** (2000) 2228.
18. *Idem.*, *J. Mater. Sci.* **36** (2001) 4977.
19. K. A. DeFRIEND and A. R. BARRON, *J. Mater. Sci.* **37** (2002) 2909.
20. C. D. JONES, M. FIDALGO, M. R. WIESNER and A. R. BARRON, *J. Membrane Sci.* **193** (2001) 175.
21. C. T. VOGELSON and A. R. BARRON, *J. Non-Cryst. Solids* **290** (2001) 216.

Received 29 April
and accepted 30 October 2002